International Journal of Thermal Sciences 195 (2024) 108666

Contents lists available at ScienceDirect

International Journal of Thermal Sciences

journal homepage: www.elsevier.com/locate/ijts

Experimental investigation of deposition patterns of citric acid modified magnetic nanofluids droplet affected by substrate temperatures

Zeyu Liu [a], Yuying Yan [b,*]

[a] Marine Engineering College, Dalian Maritime University, Dalian, 116026, China
[b] Fluids & Thermal Engineering Research Group, Faculty of Engineering, University of Nottingham, Nottingham, NG7 2RD, UK

ARTICLE INFO

Keywords:
Droplet
Deposition patterns
Nanofluids
Marangoni flow

ABSTRACT

Over the past decades, complex deposition patterns after the evaporation of particle-laden droplets spark intense interest in interpreting the formation of deposition patterns due to their numerous applications in biomedicine, ink-jet printing, biopsy, etc. This work experimentally studies the formation of deposition patterns during evaporation of the magnetic nanofluid (MNF) droplet stands on a smooth glass/hydrophobic surface at different substrate temperatures. A CCD camera mounted on the microscopy is used to capture the process of droplet evaporation. An infrared camera is applied to quantify the temperature distribution along the vapour-liquid interface of the evaporating droplet. Additionally, 3 μm sized microbeads are applied to track the flow motion of the solute inside for different temperatures. The evaporation of sessile droplets has been conducted by controlling substrate temperature, which ranges from 10 °*C* to 70 °*C*. The experimental results show that there are three distinct patterns with the increasing temperature, namely a uniform pattern, a typical 'coffee ring' pattern, and a dual ring pattern. The experimental results show that Marangoni flow becomes essential for the formation of a secondary ring pattern with increasing substrate temperatures. This study shows that controlling substrate temperature is an efficient and simple method to control the formation of the sessile droplet.

1. Introduction

Drying patterns of the droplet with suspensions are commonly observed in daily life, such as rain drop stain, scale deposition and the drying of coffee, etc. It has also been an area of scientific interest since Deegan et al. [1] found the 'coffee-ring' stain left after the evaporation of particle-laden droplet in 1997. After that, researchers carried out numerous investigations on the coffee-ring effect as shown in Fig. 1, but some outstanding questions regarding droplet evaporation still exist due to the complex internal flow and dynamics of the contact line, which is attributed to the simultaneous involvement of three phases, including vapour, liquid and solid. Additionally, the study of deposited patterns of particle-laden droplets not only plays an important role in industrial and biological applications, such as inkjet printing, coating technologies, medical testing, etc., but also is significant for cooling purposes as well as a better understanding of two-phase heat transfer [2].

For the mechanism behind the drying patterns of particle-laden droplets, the flow regime within a drying droplet is a subject of current research [4–6], especially for the deposited morphologies after the droplet evaporates. The deposited patterns are normally attributed to the complex interactions between suspensions and bulk/liquid interfaces, internal flow patterns, contact line dynamics, etc. The "coffee-ring" pattern is mainly formed by the outward capillary flow. For capillary flow, the process of evaporation follows a constant contact radius (CCR), which is pinned to the substrate surface [7]. A droplet with a contact angle below 90° has the greatest evaporative flux at the contact line. Solvents consequently transport radially from the central region of the droplet to the contact line by capillary flow, which leads to more solvents in the vicinity of the contact line. Finally, the deposited pattern forms a typical ring-like formation. Capillary flow is the dominant factor in the drying formation, but it hinders required drying patterns in practical applications, like micro-patterning of electronic devices [8], ink-jet printing [9], etc. Some investigations attempt to effectively impair the outward capillary flow of particle-laden droplet so that the ring-like pattern can be suppressed or even eliminated [10].

Marangoni flow is the other flow field inside the droplet, which can attenuate the coffee-ring effect to overcome the capillary flow [12]. It can carry the particles at the liquid-vapour interface to prevent them from migrating outward [3]. Marangoni flow is driven from the low to high surface tension (Fig. 2), which arises from two different factors. The

* Corresponding author.
E-mail address: yuying.yan@nottingham.ac.uk (Y. Yan).

https://doi.org/10.1016/j.ijthermalsci.2023.108666
Received 11 April 2023; Received in revised form 4 August 2023; Accepted 15 September 2023
Available online 21 September 2023

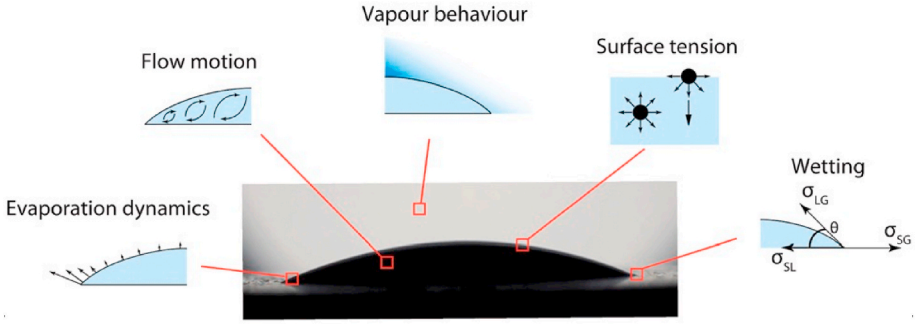

Fig. 1. Methods to address droplet wetting and evaporation [3].

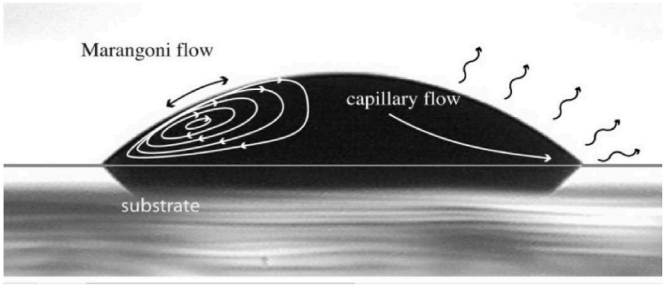

Fig. 2. Streamline plots of the flow field within an evaporating droplet for Capillary flow and Marangoni flow. The lines represent the direction of the flow [11].

first factor is the difference in local composition, also called the solute Marangoni effect [11] due to the varying concentrations of dissolved solute along the air-liquid interface. Adding surfactant changes the concentration difference along the air-liquid interface. The densely distributed surfactant molecules at the contact line decrease the local surface tension, leading to a surface tension gradient from the edge to the apex. Consequently, the colloidal particles along the air-liquid interface are transported from the contact line to the apex, which weakens the coffee-ring effect. Apart from the concentration gradients, the other factor is the temperature gradient, also called the thermal Marangoni effect. The thermal Marangoni effect changes evaporative flux over the air-liquid interface [11], leading to a surface tension difference along the air-liquid interface. However, the droplet evaporation does not always succeed in forming an internal Marangoni flow. The first reason is that the weak thermally induced Marangoni flow vanishes due to the existence of contaminants [13]. Contaminants existing along the droplet surface always make weak thermally induced Marangoni flow vanish. Additionally, evaporative cooling is highly related to the thermal conductivity of the substrate and the solution [14]. Although natural evaporation gives rise to the weak Marangoni effect, limited studies explore the effect of enhanced temperature gradients on increased Marangoni flow. Kim et al. [15] investigated the deposited patterns of both cooling and heating substrates. They found that the cooling substrate gave rise to the centrally concentrated polymer solutes, while the heating substrate enhance the evaporation, leading to a massive accumulation of solutes at the periphery. Xu and Luo [16] found the Marangoni flow in the evaporation of water droplets by fluorescent nanoparticles. Additionally, they also revealed that there was a stagnation point where surface tension, surface temperature and surface flow change direction at the droplet surface. This means that surface temperature and surface tension do not change monotonously along the air-liquid interface. Jeong et al. [17] utilised high temperature driven Marangoni flow to separate particles based on the size of particles, ranging from 100 *nm* to 15 μm. The results exhibited that particles with small sizes deposited at the outermost ring along the contact line, while particles with larger sizes accumulated at the inner rings.

Often a combination of Marangoni and Capillary flows occurs within a drop. It was determined by Kim et al. [15] that Capillary flow is stronger than Marangoni flow in the case of a heated substrate. Conversely, Marangoni flow is more prevalent on a colder substrate. This characteristic allows for the flow regime within the drop to be manipulated by controlling the temperature of the droplet.

Many experimental studies are focused on the evaporation of sessile droplets, however, the drying pattern of particle-laden droplets related to the heating substrate is scarce. Moreover, the fundamentals of droplet drying and how pattern formations related to substrate temperature are not fully understood. This work investigates the effects of a wide range of substrate temperatures (from 10 °C to 70 °C) on the deposition patterns left behind after the evaporation as well as the internal flow during the whole evaporation. This study aims to investigate the distribution of deposition patterns of MNF sessile droplets without changing chemicals. MNF sessile droplets are studied by controlling substrate temperatures, ranging from 10 °C to 70 °C. Reflection optical microscopy is applied to investigate the internal flow of the evaporation of MNF droplets and study the mechanism of deposit features of particle-laden droplets affected by substrate temperatures. To track the internal particle trajectory, 3 μm microbeads are used to analyse the flow motion inside the droplet. Additionally, an infrared camera and a CCD camera are applied to capture the surface temperature distribution and flow fields of sessile droplets, respectively.

2. Experimental methods

In this study, citric acid modified magnetic nanoparticles are selected since modification can make nanoparticles well-dispersed, which can minimise the interference of aggregation on the formation of deposition pattern of nanoparticles. Moreover, compared to other nanoparticles, modified magnetic nanoparticles will be controlled by magnetic field, which is a potential property to further control the deposition pattern of nanoparticles after understanding the mechanism of the formation of deposition pattern.

2.1. Preparation of magnetic nanofluids

Magnetic nanofluid is synthesised by using the co-precipitation technique. In a typical procedure, 24 g $FeCl_3{\cdot}6H_2O$ (≥99%, Sigma Aldrich) and 8.8 g $FeCl_2{\cdot}4H_2O$ (≥99%, Sigma Aldrich) are added into 100 mL water at first. The suspension is stirred at 50 °C and bubbled under the protection of N_2 for 2 h to remove O_2. 50 mL of ammonium hydroxide (25%, Sigma Aldrich) is then dissolved under vigorous stirring for 30 min. The black precipitate is absorbed in the bottom of the flask by a magnet and cleaned with HCl solution 5 times. 30 min later, after dumping the supernatant, the prepared precipitate is dissolved into 120 mL water by ultrasonic treatment. To cover particle surfaces with carboxyl groups, particles are coated with citric acid (≥99.5%, Sigma Aldrich) which is a small molecule with three carboxyl groups. As shown

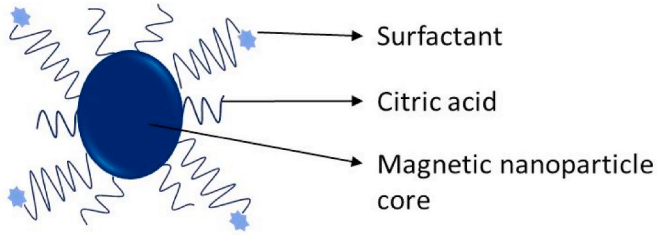

Fig. 3. The schematic structure of the modified Fe_3O_4 nanoparticle.

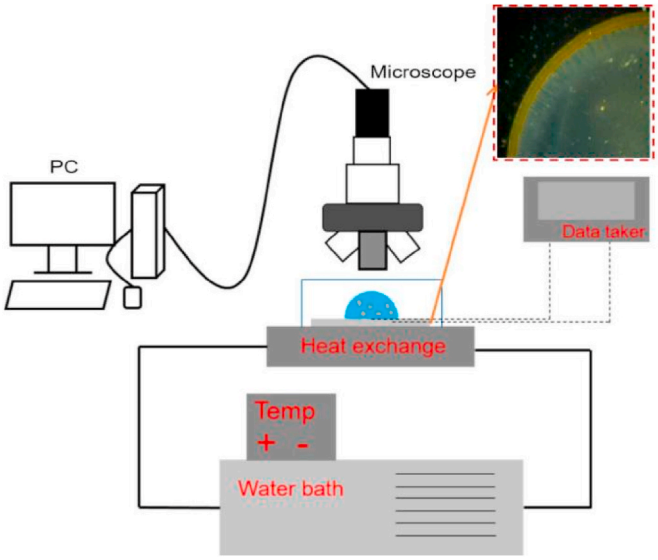

Fig. 4. Schematic setup for controlling deposition patterns of MNF droplets by controlling substrate temperatures.

in Fig. 3, citric acid can be chemically attached to the surface of a nanoparticle via the formation of a coordination bond between a metal atom and a carboxyl group, leaving one or two carboxyl groups stretching out forward into the surrounding liquid phase [18]. Finally, a certain number of coated nanoparticles in an aqueous solution are dispersed into DI water.

2.2. Experimental setup

The experimental setup is shown in Fig. 4, 0.2 wt% MNFs droplets are deposited by a micropipette (Ossila (C2001V1)) with a volume of 2 ± 0.1 μL. MNF droplets stand on the evaporation substrates, which are silicon wafers (Latech Scientific Supply Pte. Ltd.). The silicon wafers are ultrasonicated in deionised water for half an hour and are dried by compressed dry air. The modified silicon wafer is mounted on an aluminium substrate connected to a water bath (PolyScience 8006A11B Heated/Circulating Waterbath) which controls the substrate temperature ranging from 10 °C to 70 °C. Each temperature is conducted over 3 times to ensure repeatability and reliability of experimental data. Two calibrated K-type thermocouples with an accuracy of 0.1 K are inserted into the silicon wafer. Two thermocouples are located at the edge and centre to monitor the temperature uniformity respectively. During the whole evaporation process, the substrate temperature is regarded as uniform only when the temperature difference is less than 0.2 K. The test section is shielded in an open-side cylinder to prevent air turbulence disturbance. Additionally, latex microbeads, with an average diameter of 3.0 μm made of polystyrene, are conducted to understand the flow motion and mechanism. Microscopy (OPTIKA 400) mounted with a CCD camera (BASLER acA2040-90uc) is used to track the motion trajectory of particles. The surface temperature of the droplet is also recorded by an IR camera (FLIR (SC7600 M)), which is used to analyse the effect of temperature distribution over the air-liquid interface.

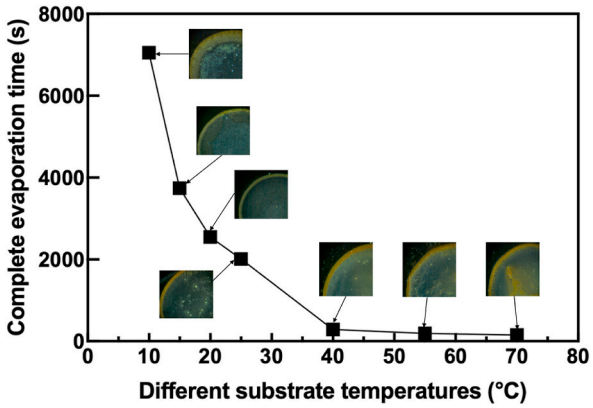

Fig. 5. Relationship between complete evaporation time (s) and different substrate temperatures (°C).

3. Results and discussion

This section investigates the effect of different substrate temperatures on drying pattern formations of MNF droplets. The substrate temperatures are classified into three stages, namely low-temperature range (10 °C, 15 °C, and 20 °C), ambient temperature (25 °C) and high-temperature range (40 °C, 55 °C, and 70 °C). Each temperature is conducted three times to ensure repeatability. Time is normalised by the evaporation lifetime, T/T_0, where T_0 refers to the completed evaporation time, and T refers to the current evaporation time. Moreover, the pattern features for MNF droplets are investigated at different substrate temperatures, and then the flow motion and analysis of different pattern formations are also discussed. According to the distribution of deposition patterns, each drying formation is divided into three regions, including the central region, gap region and edge region. The central region refers to the central area of the whole pattern, the gap region is defined as the area between the central region and the edge region. Fig. 5 shows the complete evaporation time plot for different substrate temperatures. The properties of pattern formations with different substrate temperatures are as follows.

3.1. The properties of pattern formations of MNF droplets at different substrate temperatures

3.1.1. Deposition patterns at low temperature range (10 °C, 15 °C, 20 °C)

At the low-temperature range, deposition patterns of MNF droplets exhibit a coffee ring pattern in the drying process (Fig. 6). After complete evaporation, the ring-like structure becomes more prominent as temperature increases from 10 °C to 20 °C. At 10 °C, there is a wide ring belt forming along the edge of the drying pattern. This is because at 10 °C, compared to Marangoni flow, capillary flow dominates during the evaporation process. However, the capillary flow is not strong enough to transport most magnetic nanoparticles to the edge. Size and mass both affect the path of particles [19]. Consequently, nanoparticles accumulate in the vicinity of the contact line, forming a wide ring belt as shown in Fig. 6. When substrate temperature comes to 15 °C and 20 °C, outward capillary flow still dominates, but the ring belt narrows considerably compared to that at 10 °C. The nanoparticles at the gap region distribute more uniformly. Consequently, at a low-temperature range, as the temperature increases, more nanoparticles and aggregates locate at the gap region and their distribution is more homogenous.

3.1.2. Deposition patterns at ambient temperature (25 °C)

When the substrate temperature comes to 25 °C, the ring-like

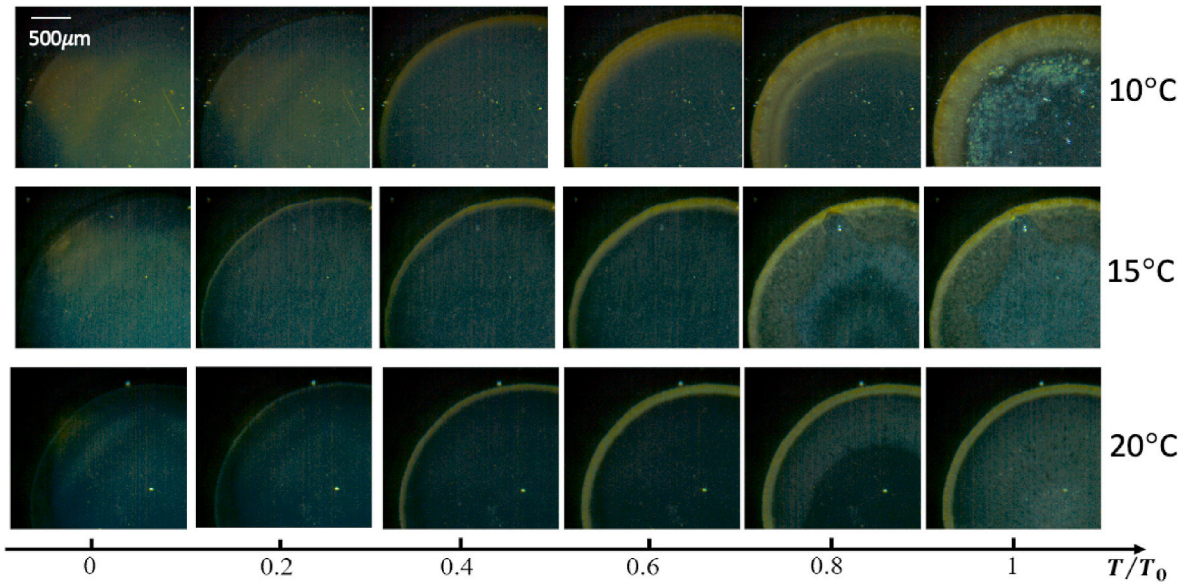

Fig. 6. Evaporation process of MNFs deposition patterns at the lowtemperature range.

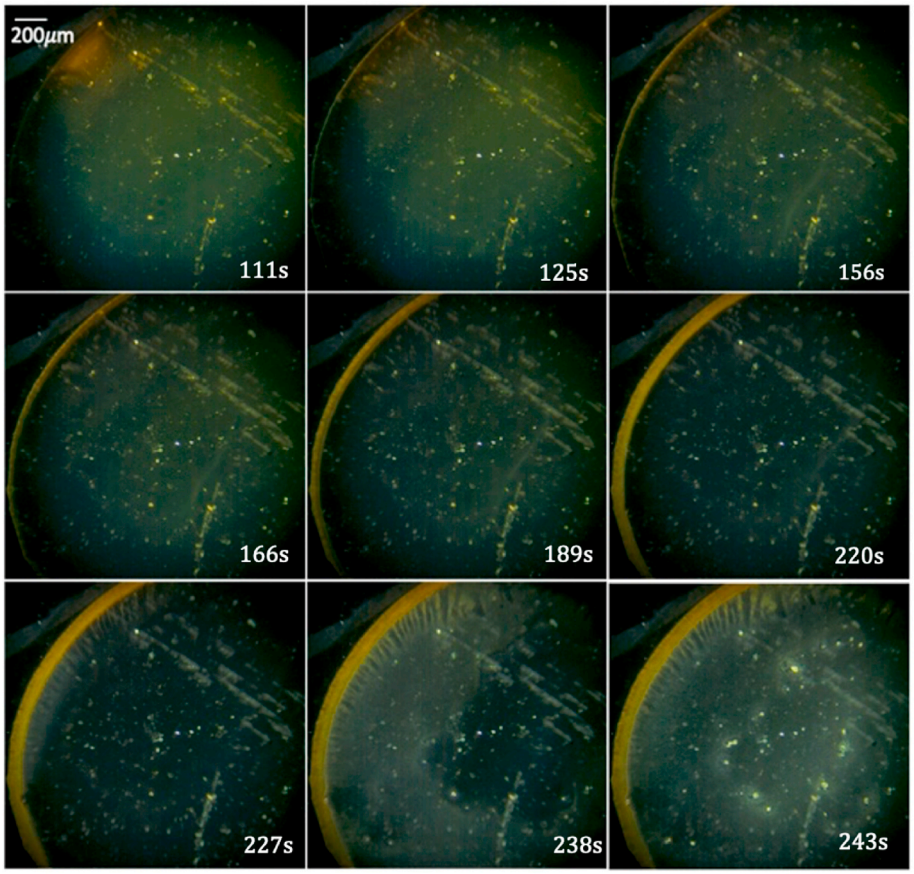

Fig. 7. Evaporation process of MNFs deposition patterns at 25 °C.

structure can also be observed at the early stage of the evaporation process as shown in Fig. 7. More magnetic nanoparticles aggregate along the contact line with the evaporation process, which increases the width of the ring belt. When it almost dries up at 227s, the ring belt along the contact line tends to move radially towards the central region, forming a finger shape pattern. After drying at 25 °C, the distribution of nanoparticles is non-uniform after evaporation, more particles aggregated in the vicinity of the contact line and there is a vague gap between the contact line and the central region.

3.1.3. Deposition patterns at high temperature range (40 °C, 55 °C, 70 °C)

At the high-temperature range, the drying formation process of the coffee ring is accelerated. At 40 °C and 55 °C, the drying pattern of MNF is similar to that at 25 °C. There is an array of finger shape patterns along

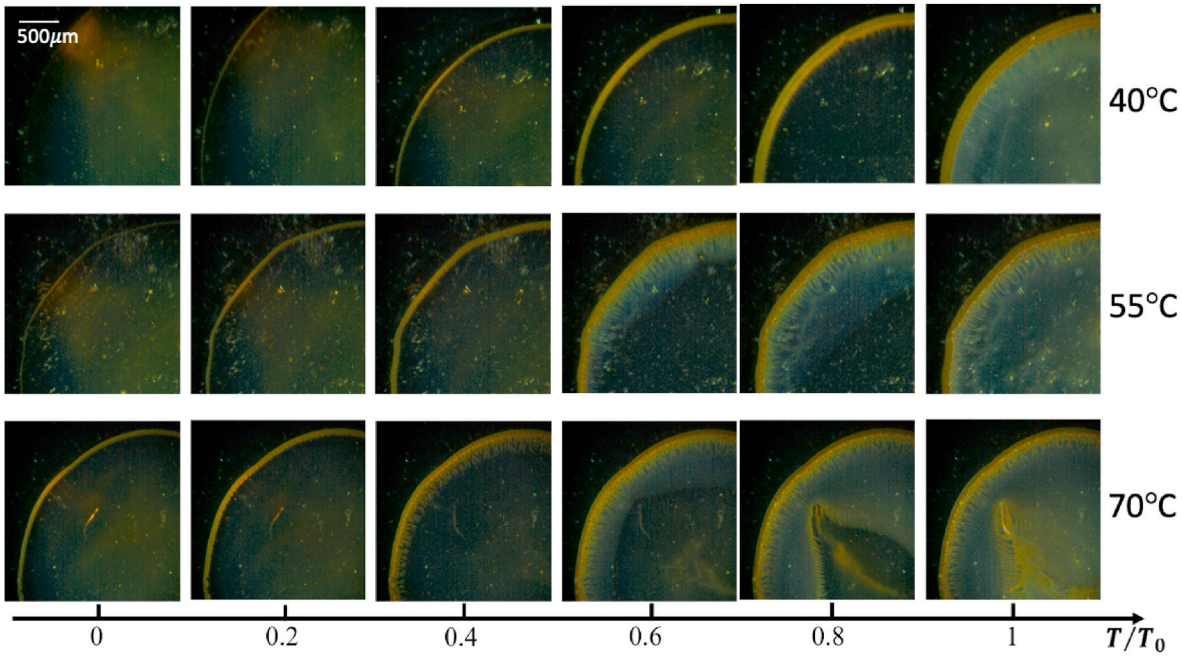

Fig. 8. Evaporation process of MNFs deposition patterns at the high-temperature range.

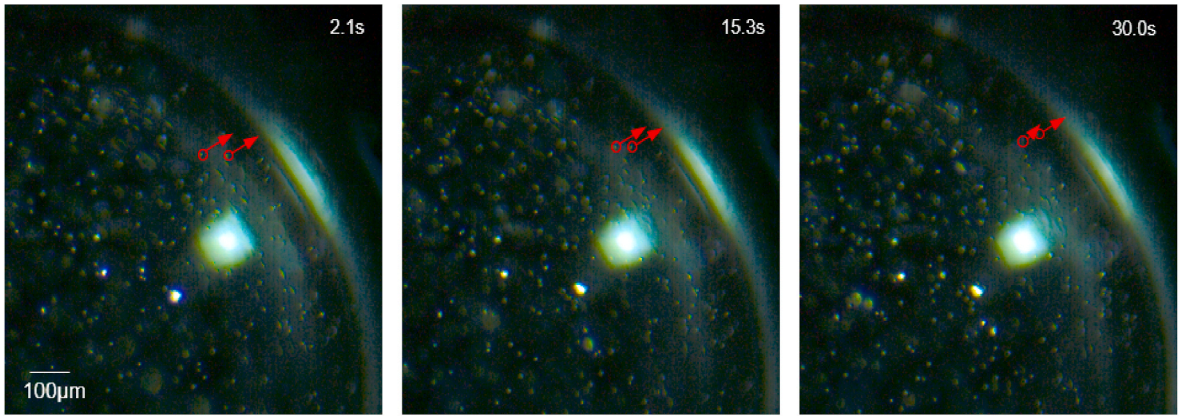

Fig. 9. Microbeads travel to the boundary along with the air-liquid interface atthe low-temperature range.

the ring-like structure in the vicinity of the contact line, pointing to the central region of MNFs. The width of the coffee ring decreases with the increase of substrate temperature. Moreover, when the substrate temperature reaches 70 °C, there is not only a finger shape pattern at the edge, but also the other finger shape pattern formed outward radially at the central region as shown in Fig. 8. This is because nanoparticles are induced to the central region by the Marangoni flow at the early stage of droplet evaporation. These induced nanoparticles are deposited into the mapped area of the substrate. As the droplet volume decreases at the final stage of the evaporation, some nanoparticles are affected by the intensive capillary flow, which forms a finger shape pattern at the central region as shown in *Fig. 8*.

3.2. Results and discussion for the mechanism of deposition patterns with substrate temperatures

To demonstrate the mechanism of pattern formations at different substrate temperatures, both the flow motion and the surface temperature distribution are analysed. In this study, 3.0 μm microbeads are used to track the trajectory of particles. The whole evaporation process is recorded by a CCD camera (BASLER acA2040-90uc) that is connected to a microscope (OPTIKA 400) from the top view. Meanwhile, a FLIR IR camera (SC7600 M) is employed to analyse the effect of surface temperature distribution over the air-liquid interface on the deposition patterns of MNF droplets. Deposition patterns are discussed from the low-temperature range to the high-temperature range.

3.2.1. Flow patterns and mechanism of microbead deposition at low-temperature range (10 °C, 15 °C, 20 °C)

At a low-temperature range, as shown in Fig. 9, solvents are transported to the contact line for the compensation of evaporated solution in the vicinity of the contact line. Mild outward transport exists since the substrate temperature is lower than the ambient temperature.

In terms of heat transfer, the surface tension gradient is dependent on the temperature gradient over the air-liquid interface, namely the Marangoni effect. When the substrate temperature is lower than the ambient temperature, surface tension decreases with the increasing temperature. Additionally, the solvents always transport from the low surface tension to the high surface tension. Fig. 10 shows the temperature distribution of droplet surface, and all thermal figures are captured at 1/5 of the droplet evaporation lifetime. The dots in thermal images are due to the reflection of IR camera and should be neglected.

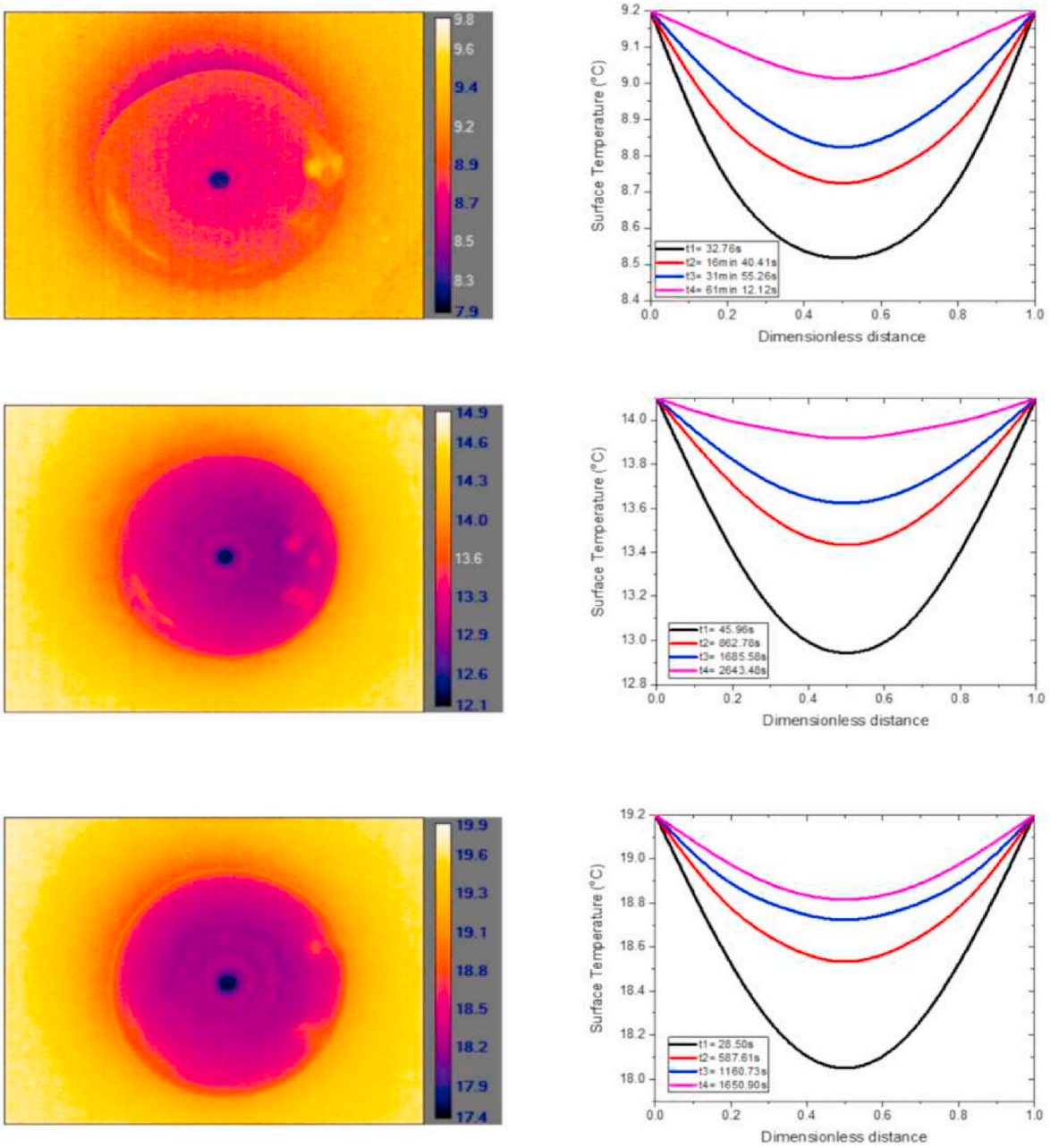

Fig. 10. Surface temperature distributions at the low-temperature range. Thermal images (left) are captured at 1/5 of evaporation time when the substrate temperature is at 10 °C, 15 °C, 20 °C respectively; subplot figures (right) present temperature distribution of droplet surface at 10 °C, 15 °C, 20 °C respectively.

According to the surface temperature distribution of the droplet, as shown in Fig. 10, it shows that temperature at the contact line is higher than that at the apex over the air-liquid interface. The maximum temperature differences along the air-liquid interface are 1.1 °C, 0.7 °C and 1.15 °C, respectively.

At 32.7s, the temperature differences are not significant compared to those at other temperatures. Thus, Marangoni flow exists at a low-temperature range but does not dominate. The solvents are transported from the contact line to the apex over the air-liquid interface, which can be proved by the flow motion as shown in Fig. 11.

Meanwhile, four particles at the central apex area are tracked as shown in Fig. 12. The trajectories of the tracked particles show that there is one vortex flow at the central region, which is driven by the Marangoni flow.

Additionally, at the final stage of evaporation (Supporting Information Video S1), three microbeads are tracked as the target particles. When the evaporative time is at 313.4s, there is nearly no movement in the radial direction. When the droplet almost dries up, as shown in Fig. 13, there are no beads transporting from the contact line to the central region, and particles barely move. This is because the temperature difference along the air-liquid interface decreases over the evaporation process. The Marangoni effect also decreases with the decreasing temperature difference, which causes particles to deposit on the substrate after the droplet dries up.

Therefore, the particle motion of droplets at low temperatures can be divided into three stages. At the early stage, particle motion is dominated by the vortex flow due to the Marangoni flow at the central region, and there is a boundary line between the central and the gap area. When some particles escape from the centre to the gap, microbeads transport along the air-liquid surface to the edge due to the Marangoni effect. Both outward transport and Marangoni flow are not intensive. As the droplet evaporates, the surface temperature difference decreases. In other

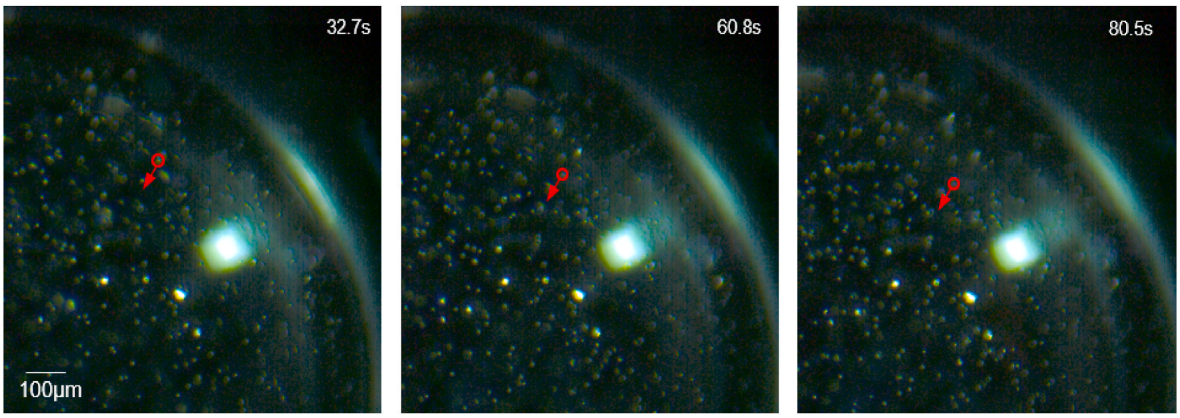

Fig. 11. Red-marked microbead travel back from the edge along air-liquidinterface at the middle stage.

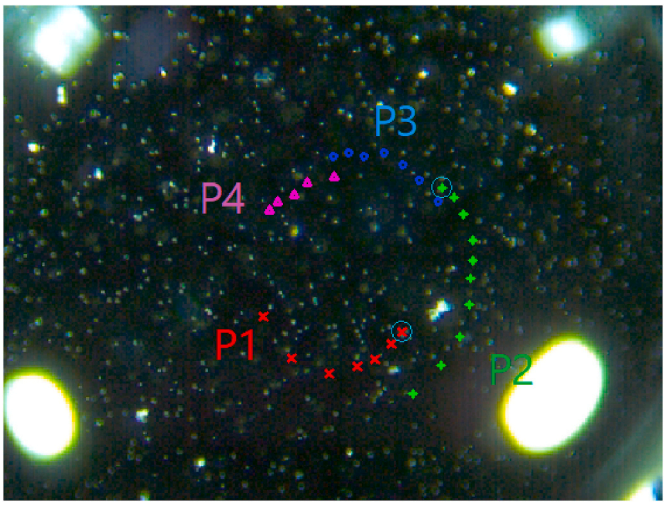

Fig. 12. Microbeads are tracked at the central area at the early stage.

words, in the middle stage, most particles are nearly in a static state. Suspended particles distribute uniformly with the decrease of the height of the droplet. At the final stage, particles travel back mildly, but the movement of particles is more violent at 20 °C than that at 10 °C. Consequently, the deposition pattern of MNF droplet exhibits more uniform with the increase of substrate temperature at low-temperature range.

3.2.2. *Flow patterns and mechanism of microbead deposition at 25 °C*

When the substrate temperature is at 25 °C, at the early stage of the evaporation process, both central and gap regions are chaotic as shown in Fig. 14. At 185.0s, the marked white particles move irregularly over time, while other marked particles at the edge region travel outwards to the contact line. In other words, capillary flow dominates the outward flow at the edge region.

According to the surface temperature distribution as shown in Fig. 15, the evaporative flux in the vicinity of the contact line is higher than that at the central region, making more solvent lost at the edge. The constant contact radius (CCR) model occupies most of the evaporative lifetime, and particles are transported to the pinned contact line for the compensation of the lost solvent.

In the second stage, at 225.3s, some particles do a spinning motion at the central region as the particle marked green (Fig. 16), while most particles follow a pair of the counter-rotating vortex (Fig. 17), which is essentially parallel to the horizontal plane. The strength of these vortices reduces over time, this is because the air-liquid interface is homogenised by the central stream as well as by the heat being transported to the cold vortex from the edge due to thermal conduction and thermal convection. Although capillary flow still dominates at the second stage as shown in Fig. 16, some particles are involved in the counter-rotating vortex as P8 (Fig. 17) when they transport to the contact line. Therefore, some particles transport back from the contact line to the central region due to Marangoni convection.

At the final stage (Supporting Information Video S2), the pair of counter-rotating vortexes disappears, and the capillary flow dominates outward transport to the contact line. As shown in Fig. 18, the particle marked red shows that some particles transport back from the contact line to the central area. This is because the MNF droplet at this stage

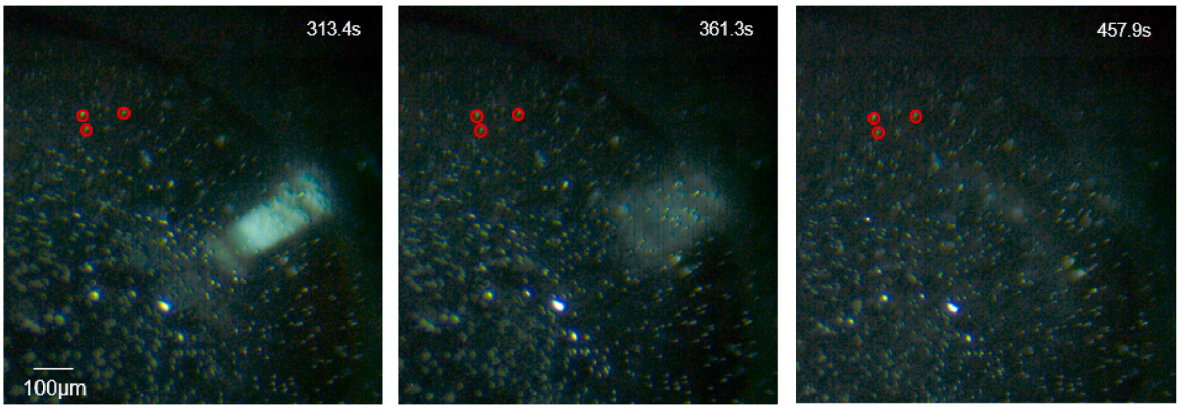

Fig. 13. Microbeads trajectories at the end of the evaporation.

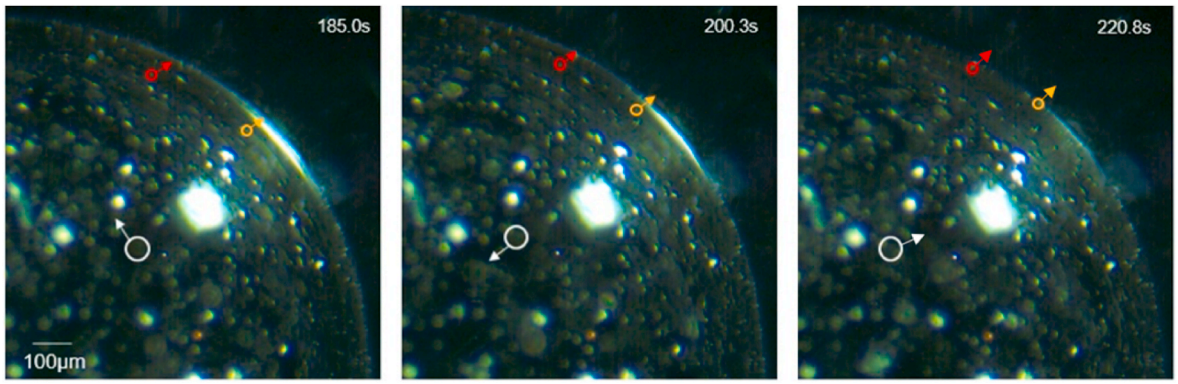

Fig. 14. Microbeads movement condition at the early stage at 25 °C.

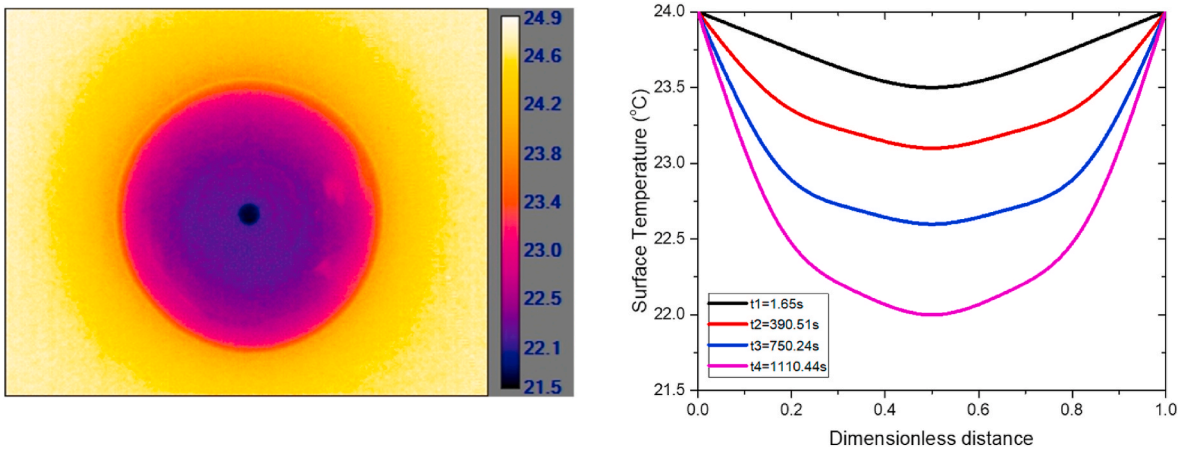

Fig. 15. Surface temperature distributions at 25 °C.

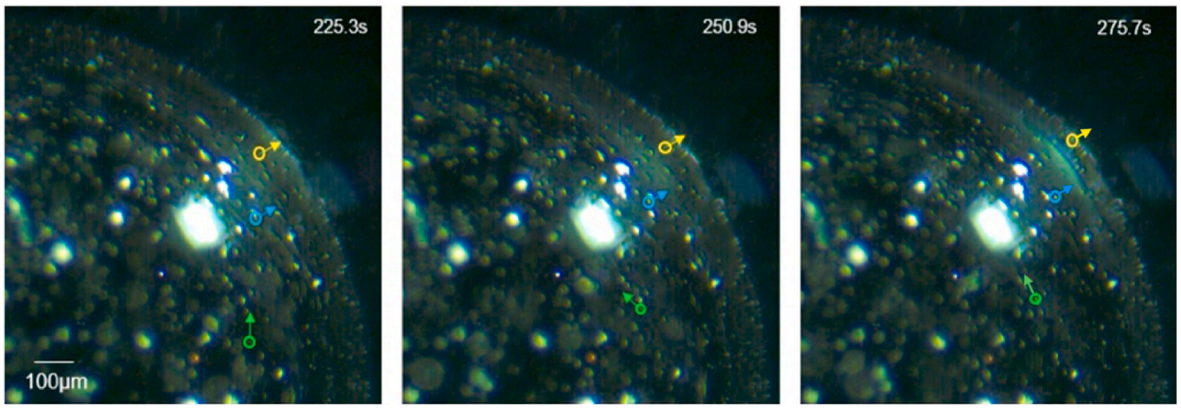

Fig. 16. Microbeads movement directions at 25 °C.

reaches a new quasi-steady equilibrium when the vortex disappears with the preferential direction of Marangoni convection. However, surface temperature difference (Fig. 15) still exists along with the air-liquid interface. Consequently, the deposition pattern forms a typical 'coffee-ring' pattern due to a dominant capillary flow. Particles at the central region are evenly distributed due to both Marangoni convection and Marangoni flow (see Fig. 19).

3.2.3. Flow patterns and mechanism of deposition at the high-temperature range (40 °C, 55 °C, 70 °C)

At a high-temperature range, the flow mode of particles is similar to that at 25 °C in the first two stages. In the early stage, the central region is chaotic. Capillary flow dominates at the gap and edge regions. The duration of the first stage is shorter than that at 25 °C and the internal flow of the droplet is more intensive. In the second stage, a pair of counter-rotating vortex flow at the central region due to the Marangoni convection. However, capillary flow dominates the edge and the gap regions. Compared to that at the ambient temperature, Marangoni flow still exists at the edge region due to a big temperature difference as shown in Fig. 23. Some particles transported to the edge are also driven back to the central region along the air-liquid interface by Marangoni flow as shown in Fig. 20.

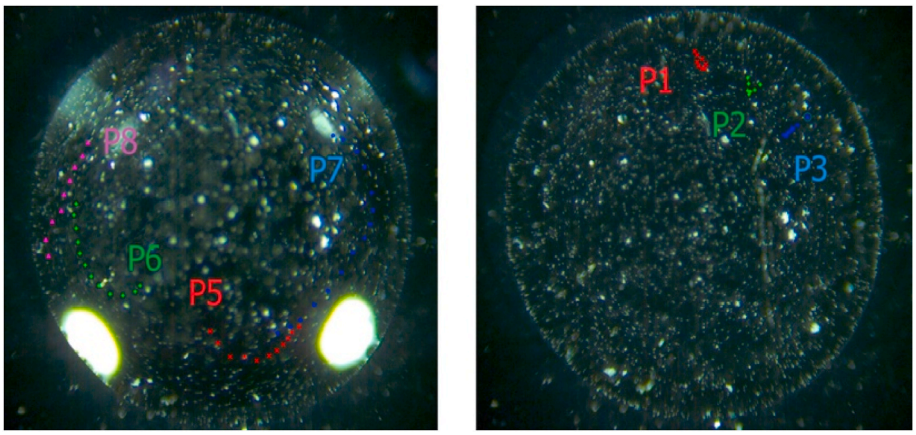

Fig. 17. Particle motion distribution at 25 °C.

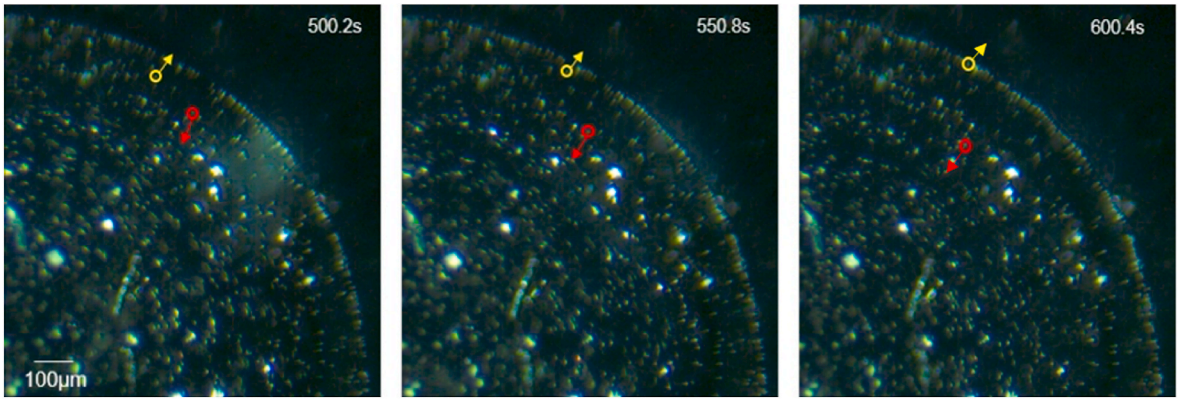

Fig. 18. Microbeads movement at the final stage at 25 °C. Flow patterns and mechanism of deposition at the high-temperature range (40 °C, 55 °C, 70 °C).

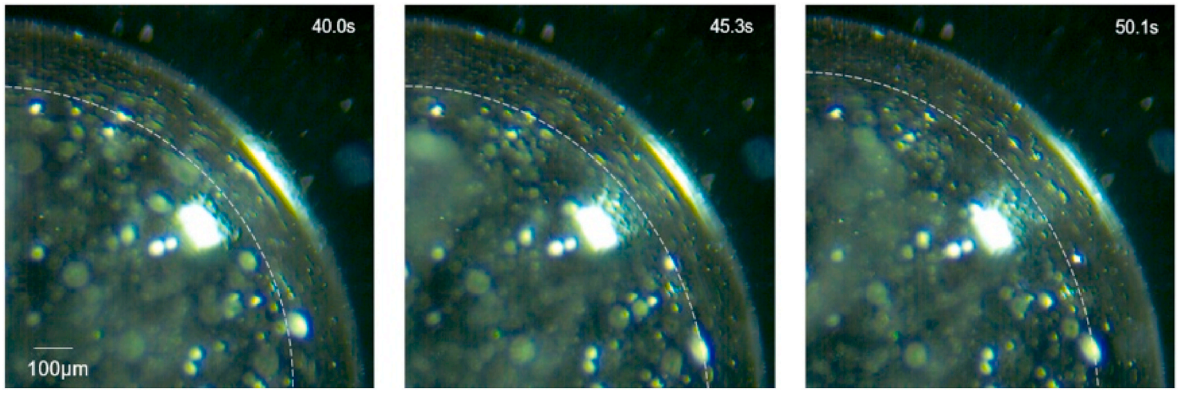

Fig. 19. Microbead movement recording at the early stage of high temperature.

At the final stage (Supporting Information Video S3), at 90.8s, the counter-rotating vortex disappears. A marked red particle transports to the edge and then flows back to the central region. Most particles move radially as shown in Fig. 21. This is because the temperature difference along the surface interface is big enough to drive particles back to the central region radially with the increasing substrate temperature. At this stage, both Marangoni flow and capillary flow contribute to the internal self-circulation flow.

When the droplet almost dries up at the final stage, the height of the droplet decreases over the evaporation time. During this period, the same amount of liquid squeezes through an area that is vanishing [20], leading to a significant increase in the particle motion speed. Therefore, when the droplet almost evaporates, both capillary flow and Marangoni flow are at the same layer close to the substrate. Particles accumulate at the gap region due to the contribution of Marangoni flow and capillary flow, eventually forming a secondary ring pattern as shown in Fig. 22.

Therefore, the whole evaporation process at the high-temperature range can be classified into three stages. In the first stage, it is similar to that at the ambient temperature, while the duration is shorter. In the second stage, both the Marangoni and the capillary flow are intense at the edge and gap regions, outward transport still dominates at this stage. Meanwhile, a pair of the counter-rotating flowing in the central region distribute particles uniformly. At the final stage, a big temperature difference along the interface makes capillary flow and Marangoni flow the

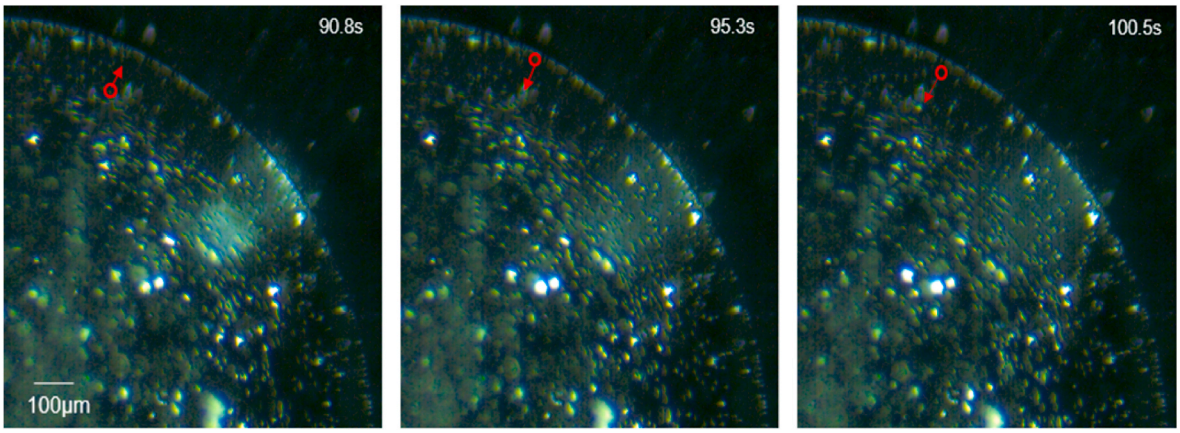

Fig. 20. Microbeads movement direction tracking at the middle stage of high temperature.

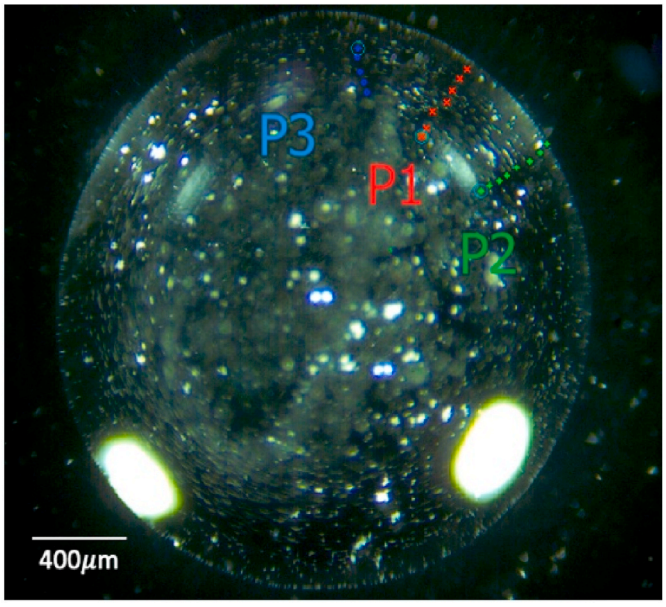

Fig. 21. Microbeads movement trajectory at the final stage of 55 °C.

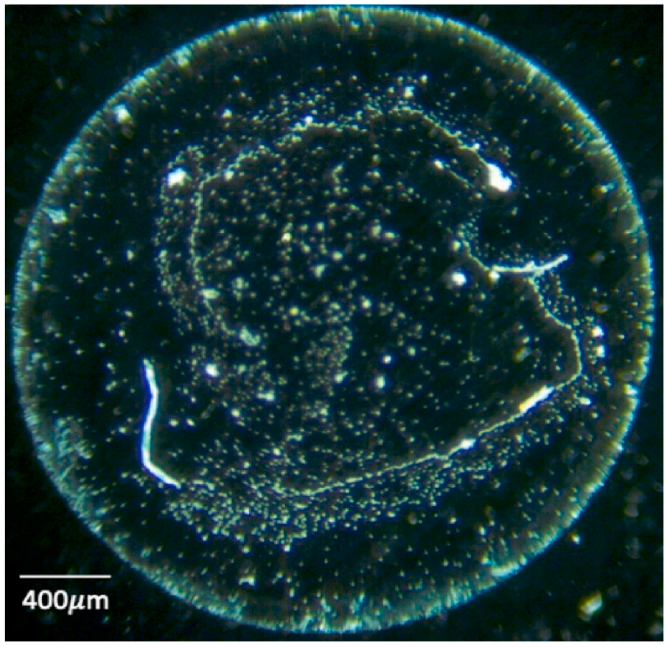

Fig. 22. The final pattern distribution of microbeads at high temperature.

two main factors for the secondary ring pattern.

4. Conclusion

In this work, the distribution of deposition patterns of MNF droplets is experimentally investigated by controlling substrate heating. The substrate temperatures are set from 10 °C to 70 °C. Drying patterns transit from the uniform pattern, the coffee ring pattern to the dual ring pattern with the increase of substrate temperatures. The capillary and the Marangoni flows play an important role in the evaporation process of MNF droplets. At the low-temperature range, the distribution of the pattern formation exhibits a uniform pattern. The Marangoni flow plays an important role in particle motion distribution. At ambient temperature, the distribution of the pattern formation exhibits a ring-like structure. Outward flow dominates the particle motion to compensate for the evaporation loss at the contact line. At the high-temperature range, the distribution of the pattern formation exhibits a dual ring pattern. Both the capillary and the Marangoni flow control the distribution of the deposition pattern during different evaporation periods. This work highlights the effect of substrate temperatures on the deposition patterns, which potentially affect the distribution of particles. For the outlook of this work, the micro-PIV technique should be further conducted to capture details at the high-temperature range; the further study should be carried out for the mechanism of variance in different deposition patterns; a standard drying method should be established to understand the effect of different drying conditions on the drying pattern formations.

There are also some limitations in this work. Microbeads can only describe the main flow of nanoparticles; CCD and IR cameras can capture limited information of droplet, more details are expected to analyse the forces inside droplet. Due to the limitations of measurement techniques in the field of droplet evaporation, more precise and suitable for the internal measurement of droplet is expected in further studies.

Declaration of competing interest

The authors declare that they have no known competing financial interests or personal relationships that could have appeared to influence the work reported in this paper.

Data availability

No data was used for the research described in the article.

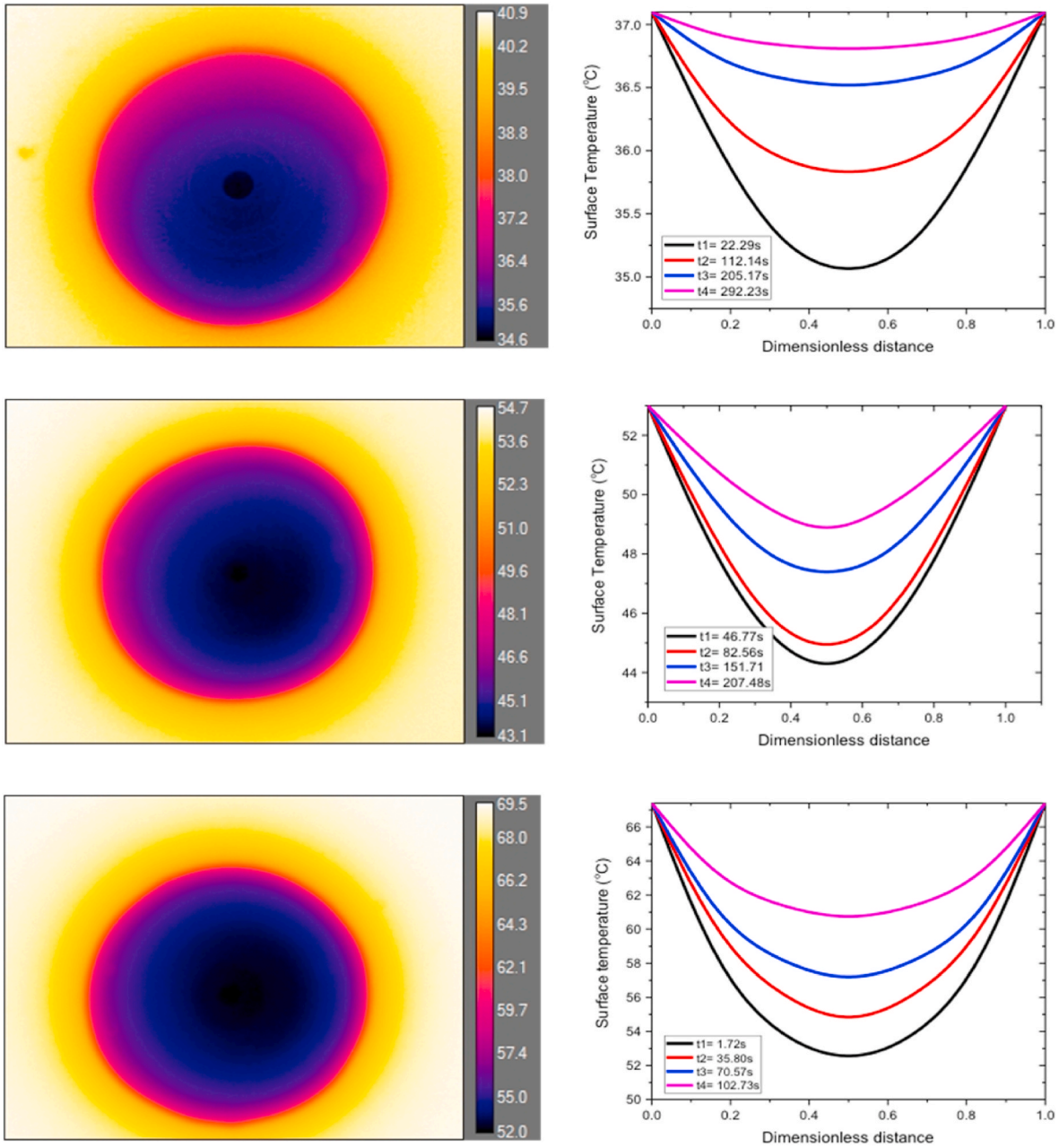

Fig. 23. Surface temperature distributions at the high-temperature range. Thermal images (left) are captured at 1/5 of evaporation time when the substrate temperature is at 40 °C, 55 °C, 70 °C respectively; subplot figures (right) present temperature distribution of droplet surface at 40 °C, 55 °C, 70 °C respectively.

Acknowledge

This work is supported by European Commision under H2020-MSCA-RISE-778104–ThermaSMART, also a doctoral degree scholarship of China Scholarship Council (CSC) under grant no. 201708060547.

Appendix A. Supplementary data

Supplementary data to this article can be found online at https://doi.org/10.1016/j.ijthermalsci.2023.108666.

References

[1] R.D. Deegan, et al., Capillary flow as the cause of ring stains from dried liquid drops, Nature 389 (1997) 827–829.
[2] J. Barber, D. Brutin, L. Tadrist, A review on boiling heat transfer enhancement with nanofluids, Nanoscale Res. Lett. 6 (1) (2011) 1–16.
[3] D. Brutin, V. Starov, Recent advances in droplet wetting and evaporation, Chem. Soc. Rev. 47 (2) (2018) 558–585.
[4] M. Parsa, et al., Effect of substrate temperature on pattern formation of nanoparticles from volatile drops, Langmuir 31 (11) (2015) 3354–3367.
[5] Z. Liu, et al., Droplet deposition pattern affected by different heating directions, Journal of Bionic Engineering 17 (4) (2020) 795–801.
[6] L. Wang, et al., Investigation on the droplet evaporation process on local heated substrates with different wettability, Heat Mass Tran. (2020) 1–13.
[7] R.D. Deegan, et al., Capillary flow as the cause of ring stains from dried liquid drops, Nature 389 (6653) (1997) 827.
[8] W. Chen, et al., In situ fabrication and characterization of graphene electronic device based on dual beam system, J. Nanosci. Nanotechnol. 15 6 (2015) 4591–4595.
[9] A. Shimoni, S. Azoubel, S. Magdassi, Inkjet printing of flexible high-performance carbon nanotube transparent conductive films by “coffee ring effect”, Nanoscale 6 (19) (2014) 11084–11089.
[10] D. Zang, et al., Evaporation of a Droplet: from physics to applications, Phys. Rep. 804 (2019) 1–56.
[11] F. Giorgiutti-Dauphiné, L. Pauchard, Drying drops, Eur. Phys. J. E 41 (3) (2018).
[12] D. Mampallil, H.B. Eral, A review on suppression and utilization of the coffee-ring effect, Adv. Colloid Interface Sci. 252 (2018) 38–54.

[13] R. Van Gaalen, et al., Competition between thermal and surfactant-induced Marangoni flow in evaporating sessile droplets, J. Colloid Interface Sci. 622 (2022) 892–903.
[14] B. Sobac, D. Brutin, Thermal effects of the substrate on water droplet evaporation, Phys. Rev. 86 (2) (2012), 021602.
[15] J.-H. Kim, et al., Polymer transports inside evaporating water droplets at various substrate temperatures, J. Phys. Chem. C 115 (31) (2011) 15375–15383.
[16] X. Xu, et al., Linear growth of colloidal rings at the edge of drying droplets, Colloids Surf. A Physicochem. Eng. Asp. 447 (2014) 28–31.
[17] H. Jeong, et al., Nanoparticle separation using Marangoni flow in evaporating droplets, in: Solid-state Sensors, Actuators and Microsystems Workshop Hilton Head Island, South Carolina, 2014.
[18] Z. Liu, et al., Experimental study of viscosity and thermal conductivity of water based Fe3O4 nanofluid with highly disaggregated particles, Case Stud. Therm. Eng. 35 (2022), 102160.
[19] M. Sommerfeld, Analysis of collision effects for turbulent gas–particle flow in a horizontal channel: Part I. Particle transport, Int. J. Multiphas. Flow 29 (4) (2003) 675–699.
[20] A.G. Marin, et al., Order-to-disorder transition in ring-shaped colloidal stains, Phys. Rev. Lett. 107 (8) (2011), 085502.